Draft version March 8, 2021
Typeset using LaTeX default style in AASTeX63

The White Dwarfs of the Old, Solar Metallicity Open Star Cluster Messier 67: Properties and Progenitors[*]

Paul A. Canton [ID],[1] Kurtis A. Williams [ID],[2] Mukremin Kilic [ID],[1] and Michael Bolte[3]

[1]*Homer L. Dodge Department of Physics and Astronomy, University of Oklahoma, 440 W. Brooks St., Norman, OK 73019, USA*
[2]*Department of Physics & Astronomy, Texas A&M University-Commerce, P.O. Box 3011, Commerce, TX, 75429-3011, USA*
[3]*UCO/Lick Observatory, University of California, 1156 High St., Santa Cruz, CA 95064, USA*

(Published 2021 March 8)

ABSTRACT

The old, solar metallicity open cluster Messier 67 has long been considered a lynchpin in the study and understanding of the structure and evolution of solar-type stars. The same is arguably true for stellar remnants – the white dwarf population of M67 provides crucial observational data for understanding and interpreting white dwarf populations and evolution. In this work, we determine the white dwarf masses and derive their progenitor star masses using high signal-to-noise spectroscopy of warm ($\gtrsim 10,000$ K) DA white dwarfs in the cluster. From this we are able to derive each white dwarf's position on the initial-final mass relation, with an average $M_{\rm WD} = 0.60 \pm 0.01 M_\odot$ and progenitor mass $M_i = 1.52 \pm 0.04 M_\odot$. These values are fully consistent with recently published linear and piecewise linear fits to the semi-empirical initial-final mass relation and provide a crucial, precise anchor point for the initial-final mass relation for solar-metallicity, low-mass stars. The mean mass of M67 white dwarfs is also consistent with the sharp narrow peak in the local field white dwarf mass distribution, indicating that a majority of recently-formed field white dwarfs come from stars with progenitor masses of $\approx 1.5\ M_\odot$. Our results enable more precise modeling of the Galactic star formation rate encoded in the field WD mass distribution.

1. INTRODUCTION

The initial-final mass relation (IFMR) is a mathematical mapping of initial mass M_i of an intermediate mass star ($\approx 0.8 - 8 M_\odot$) to the star's final mass M_f at the end of its evolution when it has become a white dwarf (WD). Early studies of the initial and final masses of stars focused on constraining mass loss (Weidemann 1977) and constraining the minimum zero age main sequence (ZAMS) mass at which a star will eventually undergo a core-collapse supernova (Romanishin & Angel 1980). Subsequently, Weidemann & Koester (1983) were the first to recognize the value of establishing an IFMR.

Much of the subsequent IFMR work has focused on covering the initial mass parameter space using WDs in open clusters (e.g., Koester & Reimers 1996; Weidemann 2000; Claver et al. 2001; Kalirai et al. 2008; Williams et al. 2009; Dobbie et al. 2009; Cummings et al. 2018; Prišegen et al. 2021), though highly useful constraints are also derived from binary field stars (e.g., Liebert et al. 2005b; Catalán et al. 2008; Andrews et al. 2015). A particularly novel approach to IFMR studies using Bayesian modeling of multiple open star clusters has been presented by Si et al. (2018); one advantage to their approach is that it considers the significant systematic impacts of cluster parameters more thoroughly than most other work has done.

Where an internally consistent set of WD and stellar evolutionary models has been employed, the dominant source of uncertainty in M_i is the age of the open cluster (e.g., Salaris et al. 2009). However, there are many other possible sources of scatter in the relation including the effects of binary evolution (e.g., Eldridge et al. 2017; Temmink et al. 2020), magnetic fields, and variable mass loss due to angular momentum (Cummings et al. 2019).

Corresponding author: Kurtis A. Williams

Kurtis.Williams@tamuc.edu

The open cluster IFMR has numerous constraints for initial masses $\gtrsim 2 M_\odot$, yet the majority of field WDs used in studies of thin disk, thick disk, and halo stellar populations (e.g., Kilic et al. 2017, 2019; Torres et al. 2021) originated from stars with initial masses $\lesssim 2 M_\odot$ (e.g., Winget et al. 1987; Kilic et al. 2017). A primary difficulty in detailing the low-mass end of the open cluster IFMR is the general lack of old ($\gtrsim 1$ Gyr) open star clusters due to their dissolution by Galactic tidal forces. A related difficulty is that the WDs in a given old open cluster span a quite narrow range in M_i; WDs from more massive stars have cooled to the point where uncertainties in the WD cooling age make derivation of the progenitor nuclear lifetimes too uncertain for precise initial mass determination.

Only a handful, though growing, number of open cluster IFMR constraints have been derived for WDs with progenitor lifetimes $\gtrsim 1$ Gyr. Kalirai et al. (2009) present WD masses in the globular cluster M4, though their metal-poor progenitors may not be an appropriate match for metal rich field stars. Kalirai et al. (2008) study the masses of WDs in the super-solar metallicity cluster NGC 6791, though the majority of these WDs are likely helium-core WDs which followed a non-canonical post main sequence evolutionary path. Thorough analysis of WDs in the open clusters NGC 7789 (age ~ 1.5 Gyr; [Fe/H] $= -0.2$) and NGC 6819 (age ~ 2.4 Gyr; [Fe/H] $= -0.04$) by Cummings et al. (2018) results in a total of five likely single WDs from both clusters combined. Most recently, Marigo et al. (2020) analyzed the IFMR in light of new WDs in the old open clusters Ruprecht 147 and NGC 752 and improved WD parameter determination methodology to present evidence for a potential "kink" in the IFMR for progenitor star masses in the range of $1.65 M_\odot \lesssim M_i \lesssim 2.1 M_\odot$. With initial masses of $\approx 1.5 M_\odot$, the WDs in M67 provide important constraints on this interpretation.

In an effort to put further constraints on the low-mass end of the IFMR, we have obtained high signal-to-noise spectroscopy for a large sample of WDs in the old open cluster Messier 67. In our first paper on the M67 WD sample (Williams et al. 2018, hereafter Paper I), we focused on the ensemble properties of the WDs. This included observational details, the WD sample selection, determination of WD cluster membership, the distribution of WD spectral types, the distribution of WD masses, potential WD remnants of blue stragglers, and a comparison of these properties to that of the WD field population. In this paper we focus on the IFMR of the M67 WD sample and how it compares and contributes to the ever-growing semi-empirical open cluster IFMR. To do so, we present details on the WD spectroscopic fitting technique used to derive WD masses and cooling ages; we discuss the careful pruning of the WD sample to include only well-measured objects that are highly likely to be cluster members that have experienced single star evolution; and we discuss the resulting measurements in light of recent developments in the open cluster IFMR. Additional commentary concerning methodology, analysis, the IFMR, and caveats are presented in Canton (2018).

2. OBSERVATIONS AND SPECTRAL ANALYSIS

WD sample selection, spectroscopic observations and spectral extraction techniques are described in detail in Paper I. In short, spectra were obtained using the Low Resolution Imaging Spectrometer (Oke et al. 1995; McCarthy et al. 1998) on the Keck I telescope. Observations employed multiple slitmasks with $1''$ wide slitlets and the 400 grooves mm^{-1}, 3400 Å blazed grism. We used the atmospheric dispersion corrector and so slitlets were not generally aligned with the parallactic angle. The onedspec and twodspec IRAF packages were used to reduce the blue channel raw data[1].

The spectroscopic fitting routine described below requires model WD spectra to be convolved with the instrumental resolution. Full-width at half-maximum (FWHM) resolutions are published on the Keck Observatory LRIS website[2] for each grism. As the spectral resolution varies slightly with slitlet placement and wavelength, we verified the FWHM where possible using the measured FWHM of the 5577Å auroral line of [O I] (Osterbrock et al. 1996). We adopt a resolution from the average of our measured FWHM and the published spectral resolution. The adopted spectral resolutions are ≈ 8.0 Å. Empirically we find that the resulting WD physical parameters change by $\leq 0.5\sigma$ in $\log g$ if the assumed spectral resolution is changed by ± 1Å; the effect is insignificant for temperature determinations.

2.1. *Spectroscopic Fitting Routine*

We derive physical parameters for each WD using the techniques and software described in Gianninas et al. (2011) and elaborated upon by Canton (2018). Briefly, we compare our spectra with the models of Bergeron et al. (1992a),

---

as updated by Bergeron et al. (1995), Liebert et al. (2005a), and Tremblay & Bergeron (2009). Using their spectral fitting routine we interpolate between models extending from 1,500 K to 140,000 K in $T_{\rm eff}$ and from 6.5 to 9.5 dex in $\log g$. We simultaneously fit the H Balmer series lines from Hβ through H9 in each spectrum.

The routine convolves the model to the input spectral resolution for each observation. The observed and model spectra are then compared by calculating a χ^2 figure of merit. A series of comparisons is performed over a grid of WD models varying in $T_{\rm eff}$ and $\log g$ with the Levenberg-Marquardt method (Press et al. 1992), an algorithm based on the path of steepest descent, to determine the physical parameters that minimize the figure of merit.

The spectroscopic fitting routine applies the mixing-length theory (ML2) of convection in one dimension for each object (Bergeron et al. 1992b). Tremblay et al. (2011b) find temperature- and gravity-dependent corrections for 3D convective effects are necessary, especially for WDs with $T_{\rm eff} \leq 15,000$ K. We therefore apply the ML2 correction functions of Tremblay et al. (2013b) and use these corrected physical parameters throughout the rest of our analysis.

As discussed in, e.g., Williams & Bolte (2007), the formal fitting errors do not account for observational scatter and other external errors (especially flux calibration). Following the discussion of Bédard et al. (2017), we have adopted the average external errors in Figure 8 of Liebert et al. (2005a) and add these in quadrature to the formal fitting errors to obtain our uncertainties in $T_{\rm eff}$ and $\log g$.

We measure the signal-to-noise ratio (S/N) in the continuum between the Hβ and Hγ lines using SPLOT in the onedspec package of IRAF. For each epoch, we use the appropriate dispersion solution and the adopted spectral resolution to convert the measured S/N per pixel to S/N per resolution element.

Normalized Balmer line fitting often results in two local minima, with one typically at a higher $T_{\rm eff}$ and lower $\log g$ than the other. We refer to these as the "hot" and "cold" solutions. In many cases visual inspection of the Balmer line fits reveals the preferred solution. In the cases where this visual inspection was not sufficient to identify the best solution, we compare the observed WD photometry (Paper I) to reddened model photometric indices derived from the calculations of Fontaine et al. (2001); Holberg & Bergeron (2006); Kowalski & Saumon (2006) and Tremblay et al. (2011a) in order to select between the two solutions. We present the physical parameters of our spectroscopic results in Table 1, and we present our best fit model Balmer line profiles plotted over the observed WD profiles for each WD in Figure 1.

In the cases of M67:WD19 and M67:WD22, the photometry does not provide clear discrimination between the two solutions. We indicate the two possible solutions by appending H (for "hot") and C (for "cold") to the object names in Table 1. We also exclude these WDs from the IFMR analysis that follows.

2.2. Notes on Individual Objects

The quality of our fits are generally excellent, but there are two primary exceptions. We exclude the following objects from further analysis for these noted reasons:

M67:WD5 — The quality of our fits for M67:WD5 are qualitatively poor despite the high signal-to-noise. In particular, the best-fitting solutions fail to replicate the depth of the Balmer line cores. This object is not a proper-motion member of Messier 67 (Paper I), so we engage in no further speculation.

M67:WD32 — We identify M67:WD32 as a DA+dM system by the presence of the TiO absorption band near 4950 Å in the red wing of Hβ. We have excluded the blended Hβ line from the fit and indicate this in Figure 1 by coloring the excluded Hβ line in green rather than red. Although the resulting fit is qualitatively good, we exclude this object from the IFMR analysis because of the possibility of binary interaction in the past.

3. THE CLUSTER IFMR

3.1. Culling the White Dwarf Sample

Construction and analysis of the semi-empirical IFMR assumes that each WD included is a coeval member of its respective open cluster and that each WD has experienced single-star evolution. Here we discuss several methods we apply to the entire WD sample in order to maximize the likelihood that these assumptions are true.

Cluster Membership — Members of an open star cluster should have nearly identical parallaxes and proper motion vectors (technically they share the same convergent point, but for distant clusters this criterion asymptotes to common proper motions).

The precision proper motion and parallax measurements of the *Gaia* early third data release (*Gaia* EDR3 Gaia Collaboration et al. 2016, 2020) are available for six M67 WDs (M67:WD1, M67:WD12, M67:WD15, M67:WD21, M67:WD25, and M67:WD32), but are otherwise of limited utility for this study. Due to their faint apparent
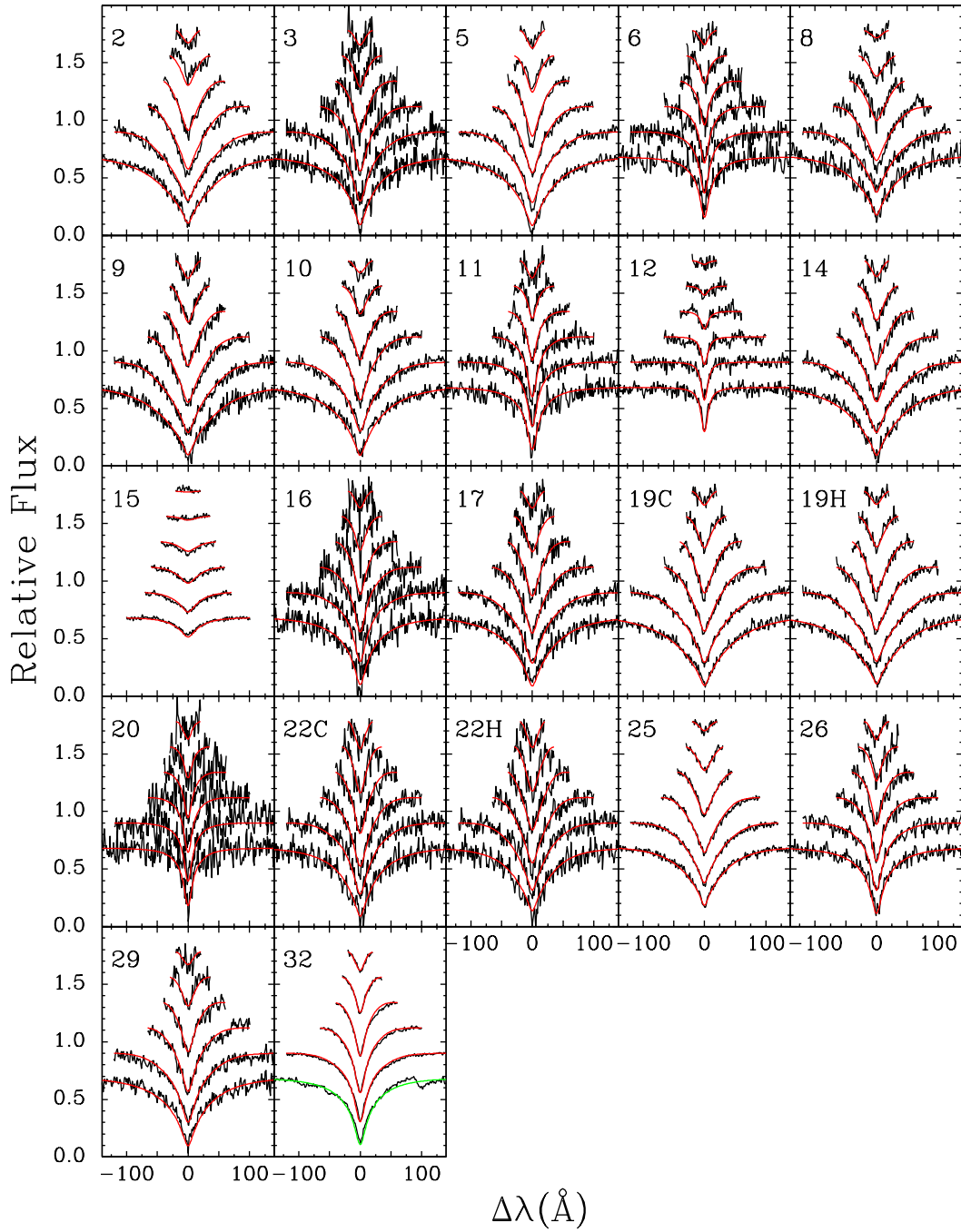
Figure 1. Normalized best-fit white dwarf models (red) overplotted on normalized Balmer-line profiles (black) for DA WDs in M67. Each panel shows the offset from line center in Ångströms plotted against normalized flux displayed from bottom (Hβ) to top (H9), with an arbitrary vertical offset in flux for clarity. The green model for Hβ in WD32 indicates that line was excluded from the fit due to contamination by a companion star (see text).

Table 1. Physical Parameters for Messier 67 White Dwarfs

Star ID	RA	Dec	$T_{\rm eff}$	$dT_{\rm eff}$	$\log g$	$d\log g$	M_f	dM_f	$\tau_{\rm cool}$	$d\tau_{\rm cool}$	S/N[a]
	J2000	J2000	K	K			$M_\odot$	$M_\odot$	log yr	log yr	
M67:WD2	8:50:39.43	11:53:26.82	14870	346	8.125	0.055	0.68	0.03	8.392	0.051	66
M67:WD3	8:50:47.60	11:43:30.04	10590	172	8.154	0.066	0.69	0.04	8.812	0.049	39
M67:WD5	8:50:52.52	11:52:06.82	11450	188	8.004	0.054	0.60	0.03	8.628	0.035	71
M67:WD6	8:50:58.61	11:45:38.79	8830	144	7.989	0.104	0.59	0.06	8.913	0.063	42
M67:WD8	8:51:01.78	11:52:34.48	20140	458	8.161	0.069	0.71	0.04	7.992	0.079	45
M67:WD9	8:51:05.31	11:43:56.66	13720	493	7.918	0.059	0.56	0.03	8.360	0.058	31
M67:WD10	8:51:08.89	11:45:44.87	11360	193	8.306	0.057	0.79	0.03	8.835	0.042	42
M67:WD11	8:51:09.14	11:45:20.21	9050	140	7.875	0.084	0.52	0.04	8.823	0.048	50
M67:WD12	8:51:09.58	11:43:52.63	7270	116	8.264	0.102	0.75	0.06	9.357	0.101	63
M67:WD14	8:51:12.11	11:52:31.32	13390	294	8.030	0.059	0.62	0.03	8.460	0.046	66
M67:WD15	8:51:19.90	11:48:40.63	53600	1041	7.629	0.066	0.54	0.02	6.241	0.042	55
M67:WD16	8:51:21.25	11:54:44.56	10030	163	8.035	0.083	0.62	0.04	8.798	0.052	34
M67:WD17	8:51:21.33	11:50:43.25	11360	201	8.036	0.060	0.62	0.03	8.656	0.041	50
M67:WD19C	8:51:24.92	11:53:56.61	13360	260	8.141	0.055	0.69	0.03	8.533	0.042	34
M67:WD19H	8:51:24.92	11:53:56.61	14950	289	8.076	0.051	0.65	0.03	8.352	0.045	34
M67:WD20	8:51:29.95	11:57:32.96	8450	149	7.687	0.141	0.42	0.06	8.809	0.062	39
M67:WD22H	8:51:37.75	11:58:43.22	15810	397	7.369	0.077	0.33	0.02	7.890	0.040	34
M67:WD22C	8:51:37.75	11:58:43.22	10460	187	7.578	0.085	0.39	0.03	8.522	0.038	34
M67:WD25	8:51:40.56	11:46:00.61	20440	308	7.977	0.045	0.61	0.02	7.768	0.057	68
M67:WD26	8:51:40.96	11:40:30.54	9580	146	7.934	0.072	0.56	0.04	8.792	0.043	68
M67:WD29	8:51:45.20	11:41:04.55	10830	178	8.252	0.062	0.75	0.04	8.854	0.047	81
M67:WD32	8:52:12.00	11:37:50.43	9780	139	7.933	0.048	0.56	0.02	8.768	0.031	220

[a]Signal-to-noise per resolution element measured across the Hβ and Hγ continuum (4500Å to 4750Å).

magnitudes, most of the WDs in our M67 sample do not appear in the *Gaia* EDR3 catalog. We queried the *Gaia* EDR3 catalog for our entire WD sample in Table 5 of Paper I, requiring positional matches within $1''.0$ and *Gaia G* magnitudes within 0.5 mag of our published g magnitudes; relaxing positional coincidence to $3''.0$ did not change the results. The matches and resulting parameters are given in Table 2.

The relevant astrometric parameters of Messier 67 as derived by Gaia Collaboration et al. (2018) are: $\varpi = 1.1325 \pm 0.0011$ mas, $\mu_{\rm RA} = -10.9737 \pm 0.0064$ mas yr^{-1}, and $\mu_{\rm Dec} = -2.9396 \pm 0.0063$ mas yr^{-1}. We determine if a WD is a proper motion member by calculating the difference between the WD and cluster proper motion vectors as follows:

$$\left(\frac{\Delta\mu}{\sigma_\mu}\right)^2 = \left(\frac{\mu_{\rm RA,WD} - \mu_{\rm RA,M67}}{\sigma_{\mu_{\rm RA,WD}}}\right)^2 + \left(\frac{\mu_{\rm Dec,WD} - \mu_{\rm Dec,M67}}{\sigma_{\mu_{\rm Dec,WD}}}\right)^2$$

The result is equivalent to a standard deviation from the cluster proper motion vector if the uncertainties are both uncorrelated and follow a gaussian distribution, and if the cluster dispersion in both parameters is zero. While none of these are technically valid assumptions, our interpretations are unlikely to change under a more rigorous analysis. The results, tabulated in Table 2, are that M67:WD12 and M67:WD32 are excluded as a cluster member by proper motion. Further, as discussed in Paper I, M67:WD15 has an apparent distance modulus significantly larger than that of M67 despite its apparent astrometric membership, so it is also excluded from the IFMR analysis.

For the WDs lacking proper motion measurements in *Gaia* EDR3, we use the proper motion memberships determined by Bellini et al. (2010) to exclude M67:WD2, M67:WD5, and M67:WD8 as cluster members, and therefore we exclude them from the IFMR analysis as well.

Table 2. Astrometric Data for M67 WDs in *Gaia* EDR3

Object	*Gaia* Source ID	ϖ	μ_{RA}	μ_{Dec}	$\Delta\mu/\sigma_\mu$	PM Member?	Notes
		mas	mas yr^{-1}	mas yr^{-1}			
WD1	604963941987041280	3.78 ± 1.86	-10.80 ± 1.63	-2.27 ± 1.46	0.47	yes	Spectral type DB
WD7	604914880575486336	$\cdots$	$\cdots$	$\cdots$	$\cdots$	$\cdots$	Spectral type DB
WD12	604911238442984704	6.96 ± 1.19	14.28 ± 1.52	-32.59 ± 0.93	35.9	no	
WD14	604922164839680384	$\cdots$	$\cdots$	$\cdots$	$\cdots$	$\cdots$	
WD15	604917698073661952	1.20 ± 0.25	-10.80 ± 0.25	-2.70 ± 0.17	1.57	yes	Photometric non-member
WD21	604898490980773888	0.98 ± 0.44	-11.48 ± 0.43	-3.43 ± 0.32	1.94	yes	Spectral type DB
WD25	604916353749379712	1.41 ± 1.20	-9.40 ± 1.45	-2.65 ± 1.50	1.10	yes	
WD30	604917079598643712	$\cdots$	$\cdots$	$\cdots$	$\cdots$	$\cdots$	Spectral type DB
WD32	604899762291059712	6.01 ± 0.87	-3.00 ± 0.93	-14.44 ± 0.75	17.5	no	DA+dM spectrum

Potential He-core WDs—— Evolved stars with core masses $\lesssim 0.45\,M_\odot$ are unable to ignite He, resulting in a He-core WD. Standard stellar evolution predicts that single stars with these low-mass cores have nuclear lifetimes significantly longer than a Hubble time, indicating that any such stars should not arise from single star evolution. WDs with masses below the He-ignition threshold are generally thought to be the product of binary evolution (e.g., Marsh et al. 1995; Brown et al. 2011), though some argue that a metallicity-dependent high mass loss rate on the red giant branch could result in He-core WDs forming via single star evolution in the present-day universe (e.g., Hansen 2005; Kalirai et al. 2007; Kilic et al. 2007). Because of this uncertainty, we exclude the potential He-core WDs M67:WD20 and M67:WD22 from the IFMR sample.

Potential Blue Straggler Remants—— We discuss in Paper I the possibility that M67:WD29 and M67:WD3 may be remnants of blue stragglers. M67:WD29 is significantly more massive ($M_{\mathrm{WD}} = 0.759 \pm 0.039 M_\odot$) than the mean mass of the cluster DAs ($\bar{M} = 0.600 \pm 0.010 M_\odot$), while M67:WD3 is mildly more massive than the mean ($M_{\mathrm{WD}} = 0.693 \pm 0.040 M_\odot$). To be conservative, we exclude both WDs from the IFMR sample, though we note that the inclusion or exclusion of M67:WD3 does not change our quantitative conclusions significantly.

Jadhav et al. (2019) claim that WD9 and WD25 are likely blue straggler progenitors based on their claim that a $1.3 M_\odot$ progenitor should create a $0.4 M_\odot$ WD. This claim is inconsistent with modern semi-empirical IFMRs (e.g., Cummings et al. 2018), so we retain these two WDs in the sample.

Overluminous WDs—— Another indication of binarity could be if a WD appears overluminous for cluster membership. While a WD in an unresolved binary may not have interacted with its companion, the analyzed spectrum will be a flux-weighted combination of the two stars' spectra, resulting in incorrect WD parameters. We therefore exclude the candidate binary WDs M67:WD10 and M67:WD19 from the IFMR sample (Paper I).

We admit that apparently single WDs in the M67 sample may have experienced binary interactions in the past (Temmink et al. 2020). This could include older double degenerate systems where a companion WD's luminosity has faded below detection limits, or WD+neutron star or WD+black hole systems that remained bound to the cluster after the supernova. However, the tight distribution of DA WD masses ($\sigma_{M_{\mathrm{DA}}} = 0.043 M_\odot$, Paper I) suggests that the impact of any such binaries is negligible on our analysis.

Remaining Sample—— After the pruning discussed above, our final sample of DA WDs in M67 used in the IFMR analysis includes seven well-measured objects: M67:WD6, M67:WD9, M67:WD14, M67:WD16, M67:WD17, M67:WD25, M67:WD26.

3.2. *Adopted Cluster Parameters*

As demonstrated by Cummings et al. (2018), when studying the IFMR it is crucial to select open cluster parameters such as distance, reddening, age, and metallicity in as consistent a manner as possible. They also demonstrate how the use of a consistent set of stellar evolutionary models both in determining these cluster parameters and in calculating the WD initial masses greatly reduces systematic scatter in the resulting IFMR. To simplify our comparisons with their

IFMR and WD data, we focus on color-magnitude diagram derived parameters based on the PARSEC 1.2S isochrones (Bressan et al. 2012; Chen et al. 2015).

Bonatto et al. (2015) use the PARSEC evolutionary models and an iterative fit to the Hess diagram for M67 to derive optimum values of the cluster parameters. Their best-fitting model has significantly subsolar metallicity, which is at odds with M67's spectroscopically determined near-solar metallicity (e.g., Pasquini et al. 2008). However, their second-ranked model more closely matches the spectroscopic metallicity, with an age of 3.542 ± 0.150 Gyr, $Z = 0.019 \pm 0.003$, $E(B-V) = 0.02 \pm 0.02$, and a distance $d = 880 \pm 20$ pc. These parameters are consistent with those used by Chen et al. (2014), who also use the PARSEC models. Even more compelling, the distance is fully consistent with the *Gaia* DR2 parallax derived for the cluster by Gaia Collaboration et al. (2018). The Bonatto et al. (2015) model-derived M67 distance corresponds to a parallax of $\varpi = 1.136 \pm 0.025$ mas, while the *Gaia* DR2 cluster parallax is $\varpi = 1.1325 \pm 0.0011$ mas.

Adopting these values, we use the CMD 3.3 interface to the PARSEC version 1.2S tracks[3] to determine that the ZAMS mass of stars currently at the start of the thermally pulsing stage of the AGB is $M_i = 1.438 \pm 0.023 \ M_\odot$.

3.3. *Calculating Initial Masses and Uncertainties*

We calculate the initial mass M_i for each WD in our final sample using the methods from Williams et al. (2009). In summary, we interpolate the cooling time $\tau_{\rm cool}$ for each WD from the WD evolutionary sequences of Fontaine et al. (2001)[4] with thick H and He layers and uniformly mixed C/O cores; this cooling time and the associated uncertainty are tabulated in Table 1. This is subtracted from the cluster age to get the progenitor star's nuclear lifetime $\tau_{\rm nuc}$; this makes the reasonable assumption that the time each star spends in the thermally-pulsing AGB and post-AGB phases of evolution are negligible compared to $\tau_{\rm cool}$ and $\tau_{\rm nuc}$. We then interpolate the PARSEC tracks to determine the ZAMS mass M_i of a star with that $\tau_{\rm nuc}$. As noted by Salaris et al. (2009), there are numerous model-dependent systematics present in such an analysis, but these are dominated by the error in the assumed cluster age.

We determine the uncertainty in our initial and final masses via a Monte Carlo method. We assume that the distribution of errors in the observed $T_{\rm eff}$ and $\log g$ of each WD are gaussian with a standard deviation given by the observational uncertainties quoted in Table 1. We then randomly draw 1000 $T_{\rm eff}$ and $\log g$ for each WD from this distribution and redetermine the M_f and M_i for each draw. The 68% envelope of the resulting distributions are tabulated as the uncertainties dM_f and dM_i. We do not consider the uncertainty in the cluster age at this point, because that will manifest itself as a systematic shift in all cluster WD M_i values and not vary randomly from WD to WD. Nonetheless, we calculate the systematic 68th percentile change in each WD's derived initial mass due to the cluster age uncertainties and present it separately with the stringent reminder that these are correlated systematic uncertainties for the entire ensemble.

The resulting M_i values and 68% uncertainty limits are given in Table 3. The remarkably tiny random uncertainties dM_i for some cluster WDs are due to the very slow change in the main sequence turnoff mass as a function of time in old stellar populations such as M67 and the fact that $\tau_{\rm cool} \ll \tau_{\rm nuc}$. For these WDs, the unaddressed systematics discussed by Salaris et al. (2009) are likely non-negligible compared to the stated uncertainties. However, the errors in M_i due to the uncertainty in the cluster age are still the overall dominant source for the cluster WDs.

As we illustrate in Williams (2020) and Canton (2018), the uncertainty distribution for individual WDs in the initial-final mass plane is usually strongly correlated and not gaussian. Given the very narrow range in M_i for the M67 WD sample, however, the correlation is dwarfed by the measurement and systematic uncertainties. We therefore present the 68% uncertainties in M_i in Table 3 without considering the correlated errors. We still emphasize the importance of the consideration of these correlated errors in any empirical IFMR studies.

4. DISCUSSION

4.1. *Comparison of M67 WDs to Existing IFMRs*

Of the multiple semi-empirical IFMRs that have been published, the analyses of Cummings et al. (2018) and Marigo et al. (2020) currently contain the largest sample of WDs analyzed in the most internally consistent manner currently possible. As our WD sample was analyzed using nearly identical methods, we compare the M67 WD sample to these IFMRs. We take the following steps in order to ensure we compare consistently derived values: (1) our M67 WD

---

[3] http://stev.oapd.inaf.it/cgi-bin/cmd

[4] Published at http://www.astro.umontreal.ca/~bergeron/CoolingModels

Table 3. Cluster White Dwarf Initial Masses

WD	M_i	$dM_{i,\mathrm{random}}$	$dM_{i,\mathrm{systematic}}$
	$(M_\odot)$	$(M_\odot)$	$(M_\odot)$
WD6	1.584	$+0.029$ -0.022	$+0.034$ -0.030
WD9	1.483	$+0.005$ -0.004	$+0.022$ -0.022
WD14	1.492	$+0.005$ -0.004	$+0.023$ -0.022
WD16	1.547	$+0.015$ -0.012	$+0.029$ -0.025
WD17	1.518	$+0.007$ -0.006	$+0.025$ -0.023
WD25	1.459	$+0.001$ -0.001	$+0.022$ -0.022
WD26	1.545	$+0.012$ -0.010	$+0.029$ -0.025

Note—Sharp-eyed readers may notice that these initial masses are systematically higher by a $\approx 0.03 M_\odot$ than in Figure 9 of Paper I. This is due to the masses in that figure having been calculated for $Z = 0.0152$, inconsistent with our adopted metallicity of $Z = 0.019$ from Bonatto et al. (2015). This error does not affect any of our conclusions from Paper I.

analysis uses spectroscopically-derived WD parameters in combination with the PARSEC 1.2S stellar evolutionary models to derive initial masses; and (2) we compare the M67 IFMR points to the WD masses and initial masses in Marigo et al. (2020) derived from spectroscopic fits alone. We recognize that Marigo et al. (2020) show that a weighted average of spectroscopic *and* photometric measurements of WD parameters result in less scatter in the semi-empirical IFMR, but we do not have photometric fits to the WD data available at this time. Our conclusions are not affected by this choice.

The comparisons are shown in Figure 2, which includes only a narrow range in M_i, and Figure 3, which displays the entire range of observed M_i. The M67 data are highly consistent with both the Cummings et al. (2018) and Marigo et al. (2020) piecewise linear IFMRs for initial masses of $\approx 1.5 M_\odot$.

In Figures 2 and 3 we also compare the M67 WDs to a linear fit of the IFMR from Canton (2018). This linear fit was generated from a reanalysis of the WD sample from Williams et al. (2009) using the Gianninas et al. (2011) methodology with the 3D corrections from Tremblay et al. (2013a) and cluster ages rederived from PARSEC isochrones. This fit also includes the M67 WDs from this work. Finally, the linear fit also includes a rudimentary consideration of the correlated errors in M_i and M_f mentioned above. While this linear fit provides a decent qualitative fit to the semi-empirical IFMR over the entire range of progenitor masses, Marigo et al. (2020) find the reduced χ^2 value of linear fits to be indicative of underfitting. Also qualitatively noticeable is the steeper slope of the data points in the $3\,M_\odot$ to $4\,M_\odot$ range as compared to a strictly linear fit, which inspired the piecewise-continuous IFMR of Cummings et al. (2018).

The M67 WDs also provide a useful sanity check for the low-mass end of the open-cluster IFMR, which lacks a significant number of points from solar-metallicity open clusters. The WDs from Cummings et al. (2018) with the lowest $M_i \approx 0.8 M_\odot$ are from the globular cluster Messier 4, while all other WDs in the relation are from open clusters with near-solar metallicities. As progenitor star metallicity affects the resultant WD mass (e.g., Romero et al. 2015), concern about the effects of the introduction of significantly sub-solar metallicity stars in the open cluster IFMR seems warranted. As the data from M67 show, any systematic effects introduced by the inclusion of Messier 4 WDs in the Cummings et al. (2018) IFMR are limited to $M_i \lesssim 1.5 M_\odot$.

4.2. *M67 WDs and the field WD population*

Since the M67 WDs in our sample arose from a small range of initial masses, and since published semi-empirical IFMRs have relatively shallow slopes over such a small range, we can reduce the uncertainty in M_i and M_f by calculating the mean values these M67 WDs: $\bar{M}_i = 1.518 \pm 0.040\,M_\odot$, and $\bar{M}_f = 0.600 \pm 0.010\,M_\odot$, where the stated
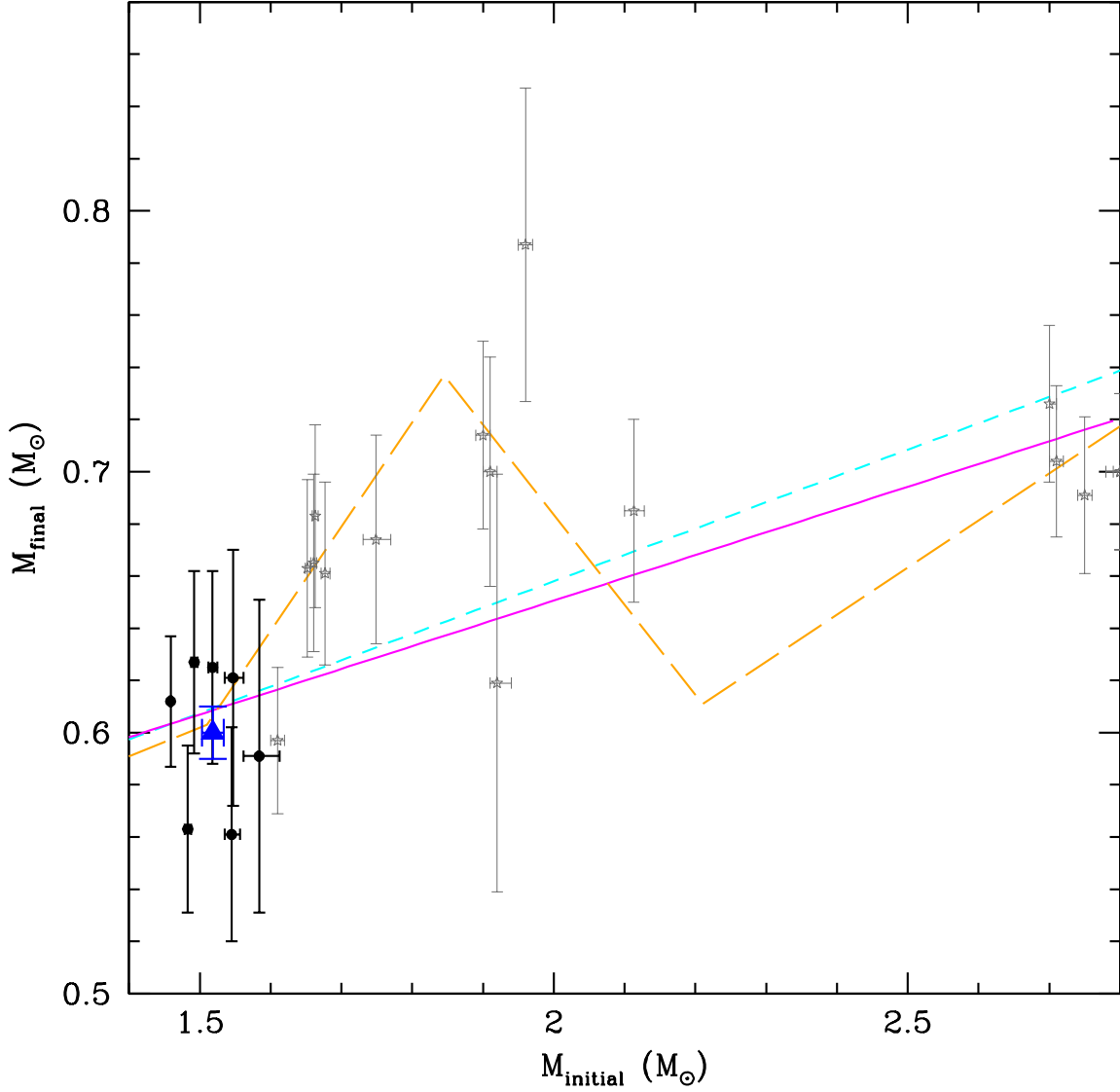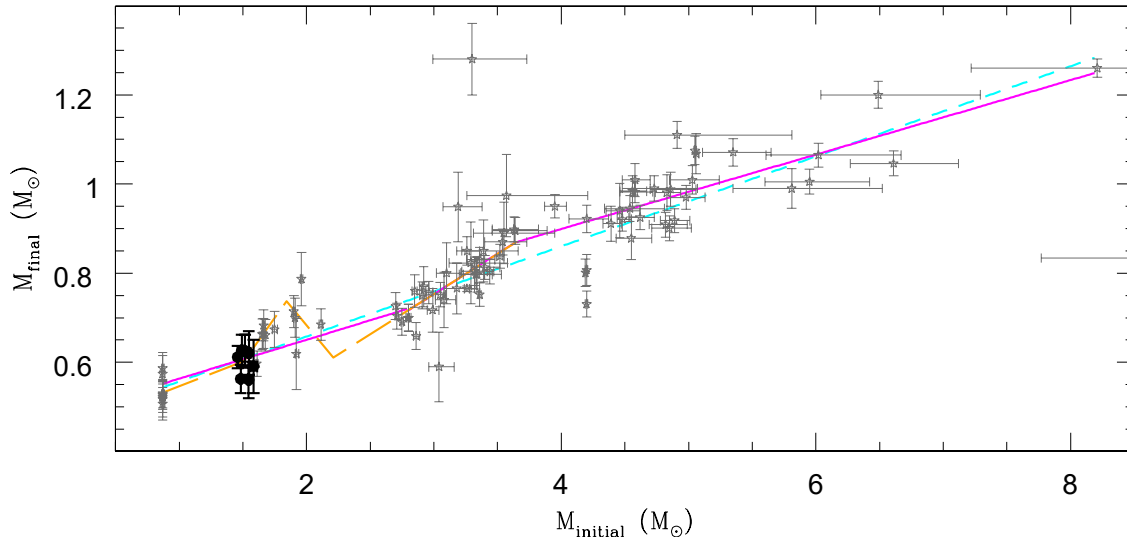
Figure 2. Comparison of the M67 WD IFMR sample to two semi-empirical IFMRs for the region with M_i between $1.4M_\odot$ and $2.8M_\odot$. Filled dark circles are the points for M67 WDs in the sample with error bars indicating the 68% uncertainty range; the large blue triangle is the mean value for these points, with error bars indicating the errors on the mean. The solid magenta line is the piecewise-continuous PARSEC IFMR from Cummings et al. (2018), the long-dashed orange line is the "kinked" IFMR proposed in Marigo et al. (2020), and the light grey stars with error bars are individual WDs from those publications. The dashed cyan line is a linear fit to the IFMR from Canton (2018). The M67 WDs are fully consistent with the functional fits from the earlier studies while providing a strong observational constraint for WDs with progenitor masses of $\approx 1.5M_\odot$.

uncertainties are the formal errors on the mean, not the standard deviation of the sample. The complete M67 WD population undoubtedly contains higher mass WDs originating from higher progenitor masses, but these WDs have cooled below our spectroscopic magnitude limits given in Williams et al. 2018.

This $\bar{M}_f$ is exceptionally close to the observed sharp peak of the field WD mass distribution of $M = 0.591M_\odot$, $\sigma = 0.035~M_\odot$ determined by Kilic et al. (2020) from within the SDSS footprint (see also Genest-Beaulieu & Bergeron

Figure 3. Comparison of the M67 WD IFMR sample to the entire semi-empirical IFMRs of Cummings et al. (2018), Marigo et al. (2020), and Canton (2018). Symbols are as in Figure 2. Again, the M67 points are consistent with (within 1σ of) the existing semi-empirical IFMRs while providing crucial constraints for $M_{\rm init} \approx 1.5 M_\odot$.

2019; Kilic et al. 2018; Tremblay et al. 2016; Gianninas et al. 2011; Falcon et al. 2010). In addition to the extremely narrow peak at 0.59 $M_\odot$, the field WD mass distribution also shows an over-abundance of $0.7 - 0.9$ $M_\odot$ WDs below $T_{\rm eff} = 10,000$ K due to a delay in their cooling from the release of latent heat of crystallization and related effects (e.g. Bauer et al. 2020; Blouin et al. 2020; Caplan et al. 2020). Given the close agreement with the M67 WD masses, we conclude that the majority of local field WDs originated from $M = 1.5$ $M_\odot$ main-sequence stars.

The field WD mass distribution encodes information about the star formation history of the Galactic disk; the mass distribution represents a convolution of the IFMR with the initial mass function and the star formation history of the disk population. Therefore, the structure of the field WD mass distribution can provide independent constraints on the star formation history of the disk, if the IFMR is reasonably well-constrained. Kilic et al. (2020) compared the mass distribution for $T_{\rm eff} \geq 10,000$ K DA WD sample against the predictions from a 10 Gyr old disk population with a constant star-formation rate, and found them to be consistent. However, they did not attempt to fit the mass distribution to derive the SFR for the disk. Several studies have suggested that the Milky Way thin disk experienced a burst of star formation $\sim 2 - 4$ Gyr ago (e.g., Cignoni et al. 2006; Rowell 2013; Bernard 2018; Mor et al. 2019). Some other recent studies of disk WDs have found weak evidence in support of this proposed star formation burst (Fantin et al. 2019; Isern 2019).

As the age of M67 is consistent with the timing of this proposed burst in star formation, and as the M67 WD masses so closely match the mass peak of the local field WD population, it seems safe to assume that the peak of the field WD mass distribution is highly consistent with what would be expected for WDs whose progenitors formed during that peak of star formation, although detailed modeling is needed to confirm whether the broader WD mass distribution is consistent with such a peak. More importantly, the tight constraints on the IFMR and WD evolution for 1.5 $M_\odot$ stars should enable more precise modeling of the Galactic star formation rate encoded in the field WD mass distribution.

ACKNOWLEDGMENTS

Facility: Keck:I (LRIS-B)

Software: IRAF (Tody 1986, 1993)

REFERENCES

Andrews, J. J., Agüeros, M. A., Gianninas, A., et al. 2015, ApJ, 815, 63

Bauer, E. B., Schwab, J., Bildsten, L., & Cheng, S. 2020, ApJ, 902, 93

Bédard, A., Bergeron, P., & Fontaine, G. 2017, ApJ, 848, 11

Bellini, A., Bedin, L. R., Piotto, G., et al. 2010, A&A, 513, A50

Bergeron, P., Saffer, R. A., & Liebert, J. 1992a, ApJ, 394, 228

Bergeron, P., Wesemael, F., & Fontaine, G. 1992b, ApJ, 387, 288

Bergeron, P., Wesemael, F., Lamontagne, R., et al. 1995, ApJ, 449, 258

Bernard, E. J. 2018, in IAU Symposium, Vol. 334, Rediscovering Our Galaxy, ed. C. Chiappini, I. Minchev, E. Starkenburg, & M. Valentini, 158–161

Blouin, S., Daligault, J., Saumon, D., Bédard, A., & Brassard, P. 2020, A&A, 640, L11

Bonatto, C., Campos, F., Kepler, S. O., & Bica, E. 2015, MNRAS, 450, 2500

Bressan, A., Marigo, P., Girardi, L., et al. 2012, MNRAS, 427, 127

Brown, J. M., Kilic, M., Brown, W. R., & Kenyon, S. J. 2011, ApJ, 730, 67

Canton, P. 2018, PhD thesis, University of Oklahoma

Caplan, M. E., Horowitz, C. J., & Cumming, A. 2020, ApJL, 902, L44

Catalán, S., Isern, J., García-Berro, E., et al. 2008, A&A, 477, 213

Chen, Y., Bressan, A., Girardi, L., et al. 2015, MNRAS, 452, 1068

Chen, Y., Girardi, L., Bressan, A., et al. 2014, MNRAS, 444, 2525

Cignoni, M., Degl'Innocenti, S., Prada Moroni, P. G., & Shore, S. N. 2006, A&A, 459, 783

Claver, C. F., Liebert, J., Bergeron, P., & Koester, D. 2001, ApJ, 563, 987

Cummings, J. D., Kalirai, J. S., Choi, J., et al. 2019, ApJL, 871, L18

Cummings, J. D., Kalirai, J. S., Tremblay, P. E., Ramirez-Ruiz, E., & Choi, J. 2018, ApJ, 866, 21

Dobbie, P. D., Napiwotzki, R., Burleigh, M. R., et al. 2009, MNRAS, 395, 2248

Eldridge, J. J., Stanway, E. R., Xiao, L., et al. 2017, PASA, 34, e058

Falcon, R. E., Winget, D. E., Montgomery, M. H., & Williams, K. A. 2010, ApJ, 712, 585

Fantin, N. J., Côté, P., McConnachie, A. W., et al. 2019, ApJ, 887, 148

Fontaine, G., Brassard, P., & Bergeron, P. 2001, PASP, 113, 409

Gaia Collaboration, Brown, A. G. A., Vallenari, A., et al. 2020, arXiv e-prints, arXiv:2012.01533

Gaia Collaboration, Prusti, T., de Bruijne, J. H. J., et al. 2016, A&A, 595, A1

Gaia Collaboration, Babusiaux, C., van Leeuwen, F., et al. 2018, A&A, 616, A10

Genest-Beaulieu, C., & Bergeron, P. 2019, ApJ, 871, 169

Gianninas, A., Bergeron, P., & Ruiz, M. T. 2011, ApJ, 743, 138

Hansen, B. M. S. 2005, ApJ, 635, 522

Holberg, J. B., & Bergeron, P. 2006, AJ, 132, 1221

Isern, J. 2019, ApJL, 878, L11

Jadhav, V. V., Sindhu, N., & Subramaniam, A. 2019, ApJ, 886, 13

Kalirai, J. S., Bergeron, P., Hansen, B. M. S., et al. 2007, ApJ, 671, 748

Kalirai, J. S., Hansen, B. M. S., Kelson, D. D., et al. 2008, ApJ, 676, 594

Kalirai, J. S., Saul Davis, D., Richer, H. B., et al. 2009, ApJ, 705, 408

Kilic, M., Bergeron, P., Dame, K., et al. 2019, MNRAS, 482, 965

Kilic, M., Bergeron, P., Kosakowski, A., et al. 2020, ApJ, 898, 84

Kilic, M., Hambly, N. C., Bergeron, P., Genest-Beaulieu, C., & Rowell, N. 2018, MNRAS, 479, L113

Kilic, M., Munn, J. A., Harris, H. C., et al. 2017, ApJ, 837, 162

Kilic, M., Stanek, K. Z., & Pinsonneault, M. H. 2007, ApJ, 671, 761

Koester, D., & Reimers, D. 1996, A&A, 313, 810

Kowalski, P. M., & Saumon, D. 2006, ApJL, 651, L137

Liebert, J., Bergeron, P., & Holberg, J. B. 2005a, ApJS, 156, 47

Liebert, J., Young, P. A., Arnett, D., Holberg, J. B., & Williams, K. A. 2005b, ApJL, 630, L69

Marigo, P., Cummings, J. D., Curtis, J. L., et al. 2020, Nature Astronomy, 4, 1102

Marsh, T. R., Dhillon, V. S., & Duck, S. R. 1995, MNRAS, 275, 828

McCarthy, J. K., Cohen, J. G., Butcher, B., et al. 1998, in Proc. SPIE, Vol. 3355, Optical Astronomical Instrumentation, ed. S. D'Odorico, 81–92

Mor, R., Robin, A. C., Figueras, F., Roca-Fàbrega, S., & Luri, X. 2019, A&A, 624, L1

Oke, J. B., Cohen, J. G., Carr, M., et al. 1995, PASP, 107, 375

Osterbrock, D. E., Fulbright, J. P., Martel, A. R., et al. 1996, PASP, 108, 277

Pasquini, L., Biazzo, K., Bonifacio, P., Randich, S., & Bedin, L. R. 2008, A&A, 489, 677

Press, W. H., Teukolsky, S. A., Vetterling, W. T., & Flannery, B. P. 1992, Numerical recipes in FORTRAN. The art of scientific computing (New York: Cambridge University Press)

Prišegen, M., Piecka, M., Faltová, N., Kajan, M., & Paunzen, E. 2021, A&A, 645, A13

Romanishin, W., & Angel, J. R. P. 1980, ApJ, 235, 992

Romero, A. D., Campos, F., & Kepler, S. O. 2015, MNRAS, 450, 3708

Rowell, N. 2013, MNRAS, 434, 1549

Salaris, M., Serenelli, A., Weiss, A., & Bertolami, M. M. 2009, The Astrophysical Journal, 692, 1013

Si, S., van Dyk, D. A., von Hippel, T., et al. 2018, MNRAS, 480, 1300

Temmink, K. D., Toonen, S., Zapartas, E., Justham, S., & Gänsicke, B. T. 2020, A&A, 636, A31

Tody, D. 1986, in Proc. SPIE, Vol. 627, Instrumentation in astronomy VI, ed. D. L. Crawford, 733

Tody, D. 1993, in Astronomical Society of the Pacific Conference Series, Vol. 52, Astronomical Data Analysis Software and Systems II, ed. R. J. Hanisch, R. J. V. Brissenden, & J. Barnes, 173

Torres, S., Rebassa-Mansergas, A., Camisassa, M. E., & Raddi, R. 2021, arXiv e-prints, arXiv:2101.03341

Tremblay, P.-E., & Bergeron, P. 2009, ApJ, 696, 1755

Tremblay, P.-E., Bergeron, P., & Gianninas, A. 2011a, ApJ, 730, 128

Tremblay, P. E., Cummings, J., Kalirai, J. S., et al. 2016, MNRAS, 461, 2100

Tremblay, P. E., Ludwig, H. G., Steffen, M., Bergeron, P., & Freytag, B. 2011b, A&A, 531, L19

Tremblay, P.-E., Ludwig, H.-G., Steffen, M., & Freytag, B. 2013a, A&A, 552, A13

Tremblay, P. E., Ludwig, H. G., Steffen, M., & Freytag, B. 2013b, A&A, 559, A104

Weidemann, V. 1977, A&A, 59, 411

—. 2000, A&A, 363, 647

Weidemann, V., & Koester, D. 1983, A&A, 121, 77

Williams, K. A. 2020, IAU Symposium, 357, 179

Williams, K. A., & Bolte, M. 2007, AJ, 133, 1490

Williams, K. A., Bolte, M., & Koester, D. 2009, ApJ, 693, 355

Williams, K. A., Canton, P. A., Bellini, A., et al. 2018, ApJ, 867, 62

Winget, D. E., Hansen, C. J., Liebert, J., et al. 1987, ApJL, 315, L77